Valence electronic structure and photofragmentation of 1,1,1,2-tetrafluoroethane (CF3-CH2F)

Kettunen, J. A.; Sankari, Anna; Partanen, L.; Urpelainen, Samuli; Kivimaeki, A.; Huttula, M.

Published in:
Physical Review A (Atomic, Molecular and Optical Physics)

DOI:
10.1103/PhysRevA.85.062703

2012

Valence electronic structure and photofragmentation of 1,1,1,2-tetrafluoroethane (CF_3-CH_2F)

J. A. Kettunen,[1,*] A. Sankari,[2] L. Partanen,[3] S. Urpelainen,[1,4] A. Kivimäki,[5] and M. Huttula[1]

[1]*Department of Physics, University of Oulu, P.O. Box 3000, FIN-90014, Finland*

[2]*Department of Synchrotron Radiation Research, Lund University, P.O. Box 118, SE-22100 Lund, Sweden*

[3]*Tampere University of Technology, P.O. Box 527, FIN-33101 Tampere, Finland*

[4]*MAX IV Laboratory, Lund University, P.O. Box 118, SE-22100 Lund, Sweden*

[5]*CNR-IOM, Laboratorio TASC, I-34149 Trieste, Italy*

(Received 15 May 2012; published 15 June 2012)

The electronic structure and fragmentation of the hydrofluorocarbon compound 1,1,1,2-tetrafluoroethane (CF_3-CH_2F) were studied using spectroscopical methods and quantum chemical calculations. Valence photoelectron spectra and the ionic fragmentation products were recorded with synchrotron radiation in the vacuum ultraviolet (VUV) region. The geometric and electronic structures of the CF_3-CH_2F molecule were calculated using the complete active space perturbation theory of second order. The calculated vertical ionization energies were used to interpret the experimental photoelectron spectrum. VUV photodissociation of the sample molecule was studied with photoelectron-photoion coincidence spectroscopy. Coincident ion yields are shown for several cations as a function of electron binding energy. The experimental data are discussed in comparison with theory and previous work.

DOI: 10.1103/PhysRevA.85.062703 PACS number(s): 34.50.Gb, 31.15.A−, 33.15.Ta, 33.15.Ry

I. INTRODUCTION

Experimental and theoretical molecular physics may be employed as a practical approach to probe the properties and behavior of atmospherically interesting molecules as they exist as positive ions under low-pressure conditions. Primarily, positive ions in the atmosphere are formed by UV and X-ray irradiation, and charged-particle impact due to solar radiation and cosmic rays [1,2]. Solar UV radiation is mostly absorbed before it reaches the lower atmosphere; however, some specific ranges of UV along with hard X-rays are able to penetrate deeper into the lower layers of the atmosphere, providing a mechanism for ionization (in addition to the energetic particle impact) of atoms, molecules, and clusters below the ionosphere [2].

The use of hydrofluorocarbons (HFCs) such as fluorinated ethanes has increased as a less ozone (O_3)-depleting alternative to chlorofluorocarbons (CFCs, commercially better known as freons) and hydrochlorofluorocarbons (HCFCs), which are planned to be phased out as a result of the Montreal Protocol on Substances That Deplete the Ozone Layer [3–8]. These synthetic gases have been used as refrigerants, propellants, blowing agents, and solvents. Their replacement is motivated by the discovery that CFC and HCFC compounds contribute significantly to stratospheric ozone depletion due to their release of catalytically acting chlorine radicals [2]. HFC compounds, in contrast, lack chlorine and their release of fluorine radicals has been seen as less damaging due to fluorine's tendency to form chemical bonds (such as HF) [9] in the upper atmosphere instead of causing ozone depletion via free fluorine radicals or other related species [4]. HFC compounds are also more readily oxidized in the atmosphere than CFCs and their stratospheric burden is approximately an order of magnitude less than that of CFCs [9]. However, the use of HCFCs and HFCs has given some reason for concern due to their toxicities and the possible adverse effects of their degradation products [2].

Recently, 1,1,1,2-tetrafluoroethane (HFC-134a) has been given attention due to its atmospheric lifetime of 14 years and modest global-warming potential (GWP) of 0.58 (20 years), which in turn will affect its global use as a refrigerant—this also applies to other halocarbons, as they are known to strongly absorb terrestrial infrared radiation [10]. As an example, in the European Union, the use of 1,1,1,2-tetrafluoroethane in automobile conditioning systems will be phased out between the years 2011 and 2017 [11]. The potential future climate contribution of HFCs has raised interest from the Montreal Protocol Parties, but the global demand for HFCs is expected to increase in developed and developing countries, especially because of a lack of regulations (see Velders *et al*. [5], Montzka *et al*. [8], and references therein).

The ion dissociation dynamics of molecules subsequent to valence and core photoionization has been of great interest to many researchers of molecular physics and physical chemistry. These phenomena have been studied with different experimental techniques, such as ion mass and electron spectroscopies [12–16]. Specific methods such as energy-scanned partial ion yields [17–20] have been used to observe the fragmentation thresholds and ion production rates, while the nature of dissociation processes has been interpreted, for example, by measuring the kinetic-energy releases (KERs) [21–23] of the participating ions. The electron-energy-dependent photoelectron-photoion coincidence (PEPICO) spectroscopy was devised to reveal a more detailed view of the underlying quantum mechanical processes, i.e., to provide a more comprehensive glimpse of the connection between specific electronic states, molecular energetics, and fragments. This experimental technique has been employed for the molecular valence and inner shells, overlapping different fields with similar interests [24–26].

In the present work, we employed time-of-flight mass spectroscopy (TOFMS), photoelectron spectroscopy (PES), and PEPICO spectroscopy to characterize the electronic

*antti.kettunen@oulu.fi

structure and fragmentation processes of 1,1,1,2-tetrafluoroethane with VUV radiation. The experimental and theoretical results are compared to previous studies by Zhou *et al*. [27,28] who have studied the photofragmentation of some HFCs, including two isomers of $C_2H_2F_4$, namely, 1,1,1,2- and 1,1,2,2-tetrafluoroethane. They have presented the breakdown diagrams for the major fragments and threshold photoelectron spectra (TPES) for both isomers. Here we present the valence photoelectron spectrum of 1,1,1,2-tetrafluoroethane.

We have also performed calculations using the MOLCAS package [29]. The computational results have been used to assign the structures observed in the experimental valence photoelectron spectrum of 1,1,1,2-tetrafluoroethane. Previous theoretical studies have included the calculation of the equilibrium geometry [30,31] and have been compared with experimental results, for example, with microwave spectroscopy by Ogata *et al*. [32]. Due to 1,1,1,2-tetrafluoroethane's atmospherical abundancy, studies reported by Papasavva *et al*. [30,31] concentrated on calculating vibrational frequencies and infrared intensities in order to estimate the global-warming potential of the molecule. The calculated results presented by Zhou *et al*. [28] included also the minimum-energy geometry of both the neutral and cationic ground state of 1,1,1,2-tetrafluoroethane, as well as enthalpies of formation of the molecule and its fragments.

In the following, the experiments shall be presented along with the calculations. The discussion is divided into sections: first, the experimental results from PES and PEPICO spectroscopy are presented; second, the details regarding fragment identification are elaborated; and, finally, the properties yielded by our calculations are compared to the experiments.

II. EXPERIMENTS

The experiments were performed at the MAX-lab (Lund, Sweden) synchrotron radiation facility on the gas-phase branch (FINEST [33]) of the I3 VUV beam line located at the MAX-III storage ring. The beam line operates in the photon-energy range of 5–50 eV. The second-order radiation effects from the monochromator are observed to be negligible at 15 eV and upward. Briefly described, the used PEPICO setup consists of a modified SES-100 hemispherical deflection analyzer (HDA) [34] with a Quantar resistive anode detector for low latency electron detection and a Wiley-McLaren-type time-of-flight mass spectrometer [35]. The TOFMS and HDA were placed facing each other, perpendicular to the photon beam axis. The so-called magic angle of 54.7° was used, defined with respect to the electric-field vector of the linearly polarized undulator radiation, corresponding to angle-independent measurements.

The photoelectron spectra (PES) were recorded with the pass energy of $E_p = 20$ eV and spectrometer slit of 0.8 mm, curved. A Gaussian full width at half maximum (FWHM) of 62.6 meV was determined for the Xe $5p$ photoelectron lines, effectively determining the experimental resolution in the electron spectra. The chamber pressure was regulated between 2×10^{-6} to 8×10^{-6} mbar. However, for the coincidence acquisitions, the amount of ionizations at the interaction region was lowered by controlling the beam-line slits and sample pressure. The photoelectron spectra are calibrated with the well-known H_2O $(1b_1)^{-1}$ photoelectron line at 12.62 eV [36], and these calibrated PES were, in turn, used to calibrate the coincidence data. The transmission calibration for the PES data was made by extracting the angle-integrated intensities of the Xe $5p$ lines, which were corrected by the $5p$ photoionization cross section and normalized to the photodiode current. The quantum efficiency of the AXUV-100 photodiode was also factored in. The Xe cross-section data were obtained from Samson and Stolte [37] and Fahlman *et al*. [38]. The transmission calibration procedure has been discussed in more detail by Niskanen *et al*. [39]. Separate TOF spectra were also recorded for photon energies between 12 and 40 eV with a step size of 1 eV.

The coincidence data were acquired by collecting what has been termed events. These coincidence events form the basic unit of our coincidence data, containing the kinetic energy of an observed electron and the time-of-flight data for zero to four coincident ions. In essence, a single coincidence-event recording is initialized by an electron-detection or a random trigger event. The TOFMS is operated in the pulsed mode so that for each real electron detection and random trigger, a TOF spectrum is obtained. In this way, electron-energy-specific spectra are obtained along with the background spectrum provided by the random triggers. With suitable normalization, the background spectrum may then be subtracted from the coincidence spectra, increasing the accuracy of the coincidence data by mitigating the impact of random coincidences. This methodology was employed in the production of the PEPICO maps and coincident ion yields (CIYs) [40] in this paper. The statistical coincidence data processing has been previously discussed in more detail [41,42]. The coincidence data were measured with the pass energy of $E_p = 100$ eV in the fixed energy mode with the 0.8 mm, curved slit. The HDA settings result in an approximated analyzer broadening of 330 meV. The PEPICO data were recorded for two separate energy windows at two different photon energies of $h\nu = 30$ and 45 eV. These two experiments cover the binding-energy ranges of approximately 12–22 eV and 22–32 eV. From now on, the lower-energy range shall be referred to as the first region and the higher-energy range shall be referred to as the second region.

The sample gas was obtained from Sigma-Aldrich. They report a typical purity of greater than 99.8%. Information about impurities was not available.

III. CALCULATIONS

A. Structure

Some problems were encountered in the previous experimental studies of the geometry of 1,1,1,2-tetrafluoroethane, which were related to the assumptions made in the interpretation of the spectroscopic or diffraction data. For example, the experimental values given by Ogata *et al*. [32], which are shown in the last column of Table I, have assumed equivalent bond lengths for all carbon-fluorine bonds in the CF_3 group. Our calculations were begun by obtaining the ground-state equilibrium geometry (see Table I and Fig. 1). The largest deviation between the previously determined experimental values and our theoretical bond lengths of this work is 0.025 Å. As for the difference between experimental and calculated

TABLE I. Bond lengths (Å) and angles (deg) in the optimized geometry of the ground state of tetrafluoroethane CF_3-CH_2F. See Fig. 1 for labeling of the atoms.

Bond, Angle	This work[a] Calc.	This work[b] Calc.	Ref. [28] Calc.	Ref. [30] Calc.	Ref. [32] Expt.
C_1–C_2	1.513	1.513	1.507	1.508	1.525
C_1–F_3	1.317	1.317	1.352	1.353	1.336
C_1–F_4	1.311	1.311	1.344	1.346	1.336
C_1–F_5	1.311	1.311	1.344	1.346	1.336
C_2–F_6	1.361	1.361	1.382	1.382	1.345
C_2–H_7	1.080	1.087	1.092	1.088	1.090
C_2–H_8	1.101	1.087	1.092	1.088	1.090
∠ (F_3-C_1-C_2)	108.8	108.8	109.1	109.1	108.9
∠ (F_3-C_1-F_4)	108.0	108.0	108.2	108.2	
∠ (F_4-C_1-F_5)	108.0	108.0	108.0	108.0	107.8
∠ (F_4-C_1-C_2)	111.9	111.9	111.6	111.6	112.1
∠ (F_6-C_2-C_1)	109.6	109.7	108.5	108.7	109.7
∠ (F_6-C_2-H_7)	109.5	109.4	109.9	109.9	106.1
∠ (H_7-C_2-H_8)	110.4	110.2	110.4	110.3	108.9
∠ (C_1-C_2-H_7)	109.3	109.0	109.1	108.9	112.9

[a]Without symmetry adaptation.
[b]With symmetry adaptation.

angles, the largest can be found from the C_1-C_2-H_7 angle (3.9°). This is most probably due to the assumptions made in the experimental data analysis.

The structural parameters were obtained by a geometry optimization performed using the MOLCAS package at the complete active space perturbation theory of second order (CASPT2) level of theory [43,44] using the large atomic natural orbitals basis set (ANO-L-VTZP). The same basis set was used in all calculations presented in this paper. Previous calculations and the interpretation of experimental results have assumed a C_s symmetry of the molecule. That is, fluorine atoms F_4 and F_5 as well as the hydrogens H_7 and H_8 are equal with respect to the plane spanned by F_3, C_1, C_2, and F_6.

We would like to point out that our geometry optimization was performed without symmetry requirements and the result was slightly asymmetric, as can be seen from the hydrogen bond lengths given in the second column of Table I. The optimized geometry is very close to a staggered structure with C_s symmetry, and therefore we made the molecule symmetric

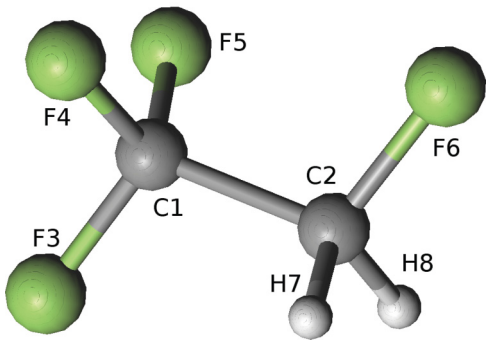

FIG. 1. (Color online) Optimized geometry for CF_3-CH_2F in the ground state. The atomic labels refer to those used in the text and in Table I.

(the resulting values, used in the energy calculations, are given in the third column of Table I). Only bond lengths for the hydrogens were changed and a minor adjustment of the bond angles in the CH_2F group was made. This improved the match between the calculated and experimental energies in the valence photoelectron spectrum.

For comparison, Table I also lists the parameters from a previous theoretical study by Papasavva *et al*. [30] obtained at the MP2/6-31G** level of theory, as well as the more recent ones by Zhou *et al*. [28] at the MP2(full)/6-31G(d) level of theory. Values between these two previous, similar calculations do not differ much, and the largest differences between our values and the previously calculated values can be found from the C_1–F_4 (or C_1–F_5) bond length (0.035 Å) and the F_6-C_2-C_1 angle (1.2°). All of these calculations suggest that the C_1–F_3 bond is longer than the two other C_1–F bonds, and that the C_2–F_6 bond is the longest of them all. Our calculations predict somewhat shorter C–F bonds and a longer C–C bond than previous calculations, but there are no significant differences in the computed angles.

B. Ionization energies

In order to identify the origin of observed structures in the photoelectron spectrum, ionization energies from the highest-lying molecular orbitals (MOs) were computed. Absorption of the photon and emission of the electron are assumed to happen in a time scale which is shorter than the time needed for the nuclei to rearrange themselves, and hence the Born-Oppenheimer approximation was applied. The symmetry-adapted geometry obtained for the ground state (see Table I) was used to calculate the vertical ionization energies (VIEs) for the 1,1,1,2-tetrafluoroethane ion.

The goal was to obtain energies for configurations differing by only one electron from the ground state (the dipole operator is a one-electron operator). For this purpose, the restricted active space (RAS) approach [45] was employed in energy calculations. The nine innermost molecular orbitals of a' symmetry and the two of a'' symmetry occupied the inactive space, and the rest of eight a' and six a'' orbitals were placed on RAS 1 space where they were allowed to have only one hole. Energies were then optimized for the first eight levels of a' symmetry and six levels of a'' symmetry by a state-average restricted active space self-consistent field (SA-RASSCF) method [46]. Electronic energies, including the dynamical correlation, are given in the third column of Table II and are the result of a multistate second-order perturbation theory (MS-CASPT2) [43,44] step applied after the RASSCF step for each symmetry.

IV. RESULTS AND DISCUSSION

A. The photoelectron spectra

PES measured at photon energies of $h\nu = 30$ and 50 eV are shown in Fig. 2. Both Figs. 2(a) and 2(b) have been corrected for the transmission of the HDA with the procedure explained in Sec. II. The experimentally detected bands have been labeled with an index running from 1 to 8 in increasing binding energy—later these indices will be referred to when considering the fragmentations subsequent to different photoionized

TABLE II. Calculated and experimentally determined VIEs (eV).

Band	Orbital	Calc.	Expt.
1	$17a'$	13.96	13.96
2	$8a''$	15.74	15.56
	$16a'$	15.91	
	$7a''$	16.37	
3	$6a''$	16.85	17.17
	$15a'$	16.98	
	$14a'$	17.17	
4	$5a''$	18.21	17.99
	$13a'$	18.78	
5	$4a''$	19.98	19.98
	$12a'$	20.59	20.70
	$11a'$	21.16	
6	$3a''$	22.23	22.99
7	$10a'$	23.57	25.88

states. Due to the typical energetical overlaps observed in valence spectra, the valence photoelectron spectrum of the residual gas background is also displayed in Fig. 2(a). The theoretically predicted VIEs are added as vertical bars. For reference, VIEs are also listed in Table II. As can be seen from Figs. 2(a) and 2(b), reasonable agreement is found between the theoretical VIEs and observed bands. The theoretical energies have been shifted by a constant value to match better with the experiment. After this shift, the agreement is seen to match to a good degree so that the assignment of the band structure can be attempted. In Fig. 2(b), the inner valence structure is observed to rise after a binding energy (BE) of 30 eV.

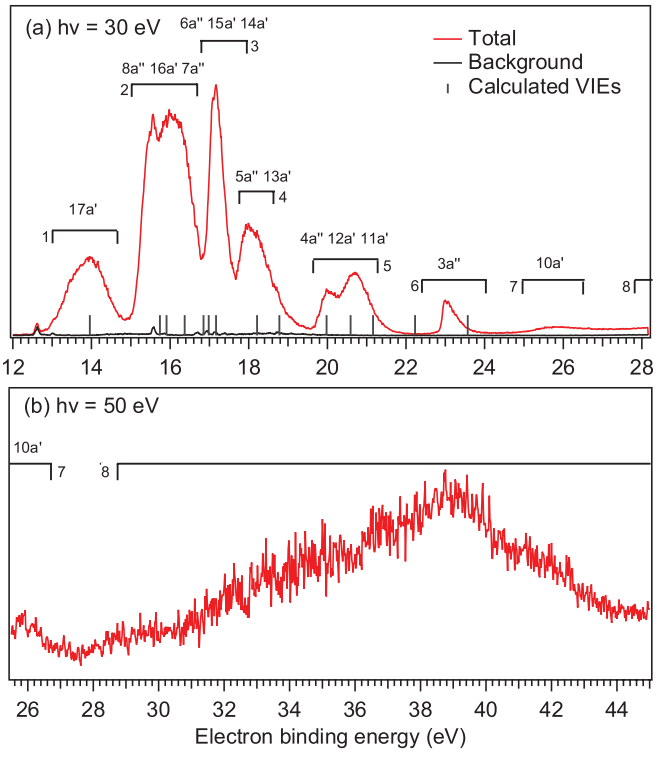

FIG. 2. (Color online) The photoelectron spectra of the 1,1,1,2-tetrafluoroethane valence. The spectra have been calibrated for the analyzer transmission. The absolute binding-energy scale in spectra (a) and (b) has been calibrated with H_2O and N_2 photoelectron lines. The orbital label refers to the respective photoionized MOs, and in turn the MOs are grouped into their respective bands. The vertical bars are the shifted theoretical VIEs obtained with MS-CASPT2 calculations. The intensities of the vertical bars are arbitrary.

Due to heavy overlap within the bands, an exact VIE determination for the experimentally observed ionized states is rather difficult. According to our calculations, the electronic configuration of 1,1,1,2-tetrafluoroethane is $(10a')^2(3a'')^2(11a')^2(12a')^2(4a'')^2(13a')^2(5a'')^2(14a')^2(15a')^2(6a'')^2(7a'')^2(16a')^2(8a'')^2(17a')^2$, which is in accordance with the valence configuration given by Zhou *et al.* [28], with the exception of the $16a'$ and $7a''$ labels switching places. Due to this inconsistency and the problematic nature of accurate VIE determination for overlapping ionized states, the MO labeling of the band structures is considered tentative.

Justified by the calculations, previous work [28], and appearance, band 1 is considered to contain the first excited state subsequent to outermost MO ionization, $(17a')^{-1}$. The theoretical adiabatic ionization energy (AIE) and the observed AIE have been reported [28] at 12.25 eV and 12.64 $\pm$ 0.05 eV, respectively, where the apparent discrepancy has been explained by unfavorable Franck-Condon (FC) factors. The shape of band 1 (Fig. 2) displays a slow rise, which indicates a low FC factor between the lowest vibrational states. This, in turn, suggests heavy bond-length dependency on the involved orbital. In previous work [28], experimental and theoretical VIEs have been determined at 14.01 $\pm$ 0.05 eV and 13.96 eV, respectively, whereas the electron spectrum of Fig. 2(a) provides a VIE of 13.96 eV within the first structure observed.

Band 2 is observed to contain contributions from at least two different ionic states, $(8a'')^{-1}$ and $(16a')^{-1}$, and likely from $(7a'')^{-1}$ as well. The lower-energy side of the band structure indicates the removal of a nonbonding electron as a fast rise towards the VIE is observed. The high-energy side, however, displays an unresolved vibrational envelope, where clear state separation is not observed.

Band 3 is sharper than the others, but shows slight asymmetry on the high binding-energy side, which is likely due to vanishing FC factors. The MO characteristics for the states $(6a'')^{-1}$ and $(15a')^{-1}$ are seen to contain a fluorine lone-pair nature, which, due to possible single bond fission, may explain the third band's appearance.

Band 4 displays clear asymmetry towards the higher-energy end, indicating strongly that it contains at least two different, overlapping states, here labeled as $(5a'')^{-1}$ and $(13a')^{-1}$.

Band 5 is assigned to the $(4a'')^{-1}$, $(12a')^{-1}$, and $(11a')^{-1}$ states on an energetical basis. Two clearly separated structures are observed, and the higher-energy side displays features, which indicates contribution from a third state.

According to the calculations, band 6 is likely to contain the $(3a'')^{-1}$ state, which is heavily delocalized with its constituents being a mix of almost all bonds. In contrast to band 1, band 6 reveals (see Fig. 6) another type of traditional PES shape, where the band begins with a sharp rise and then decays clearly. This indicates a substantial amount of lowest vibrational state excitation into a bound ionic state.

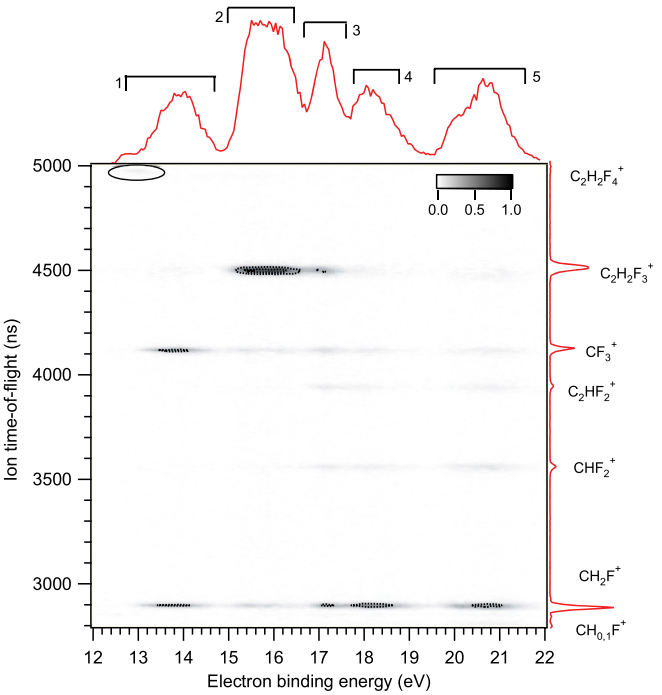

FIG. 3. (Color online) The first region PEPICO map of 1,1,1,2-tetrafluoroethane ($h\nu = 30$ eV). The dashed contour lines have been set at 33% and 66% of the maximum intensity. The encircled area indicates the extremely weak trace of the parent ion.

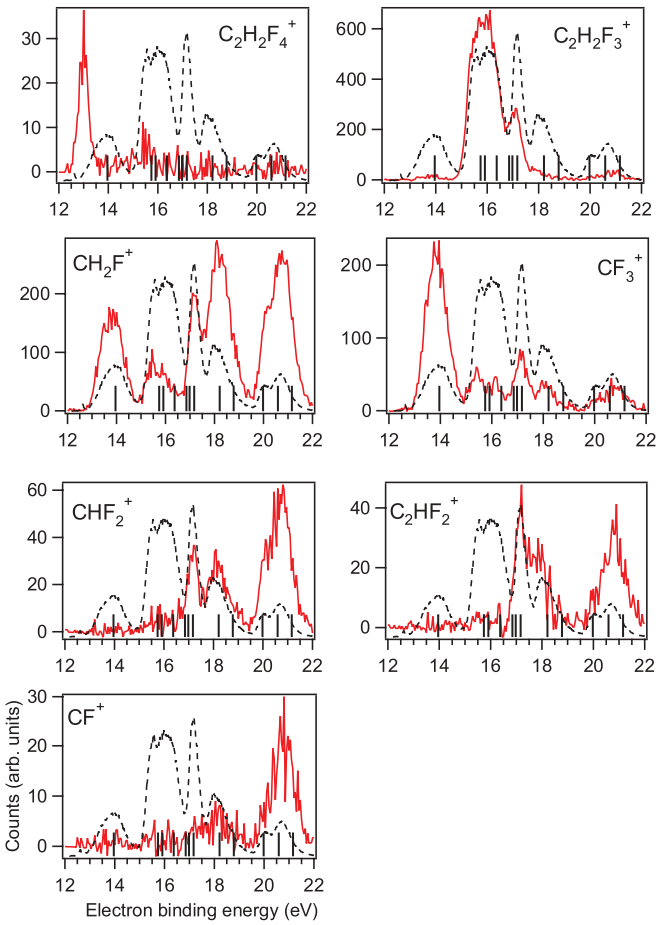

FIG. 4. (Color online) Coincident ion yields (CIYs) for the most abundant fragments observed subsequent to CF_3-CH_2F photoionization ($h\nu = 30$ eV) within the first PEPICO region. The yields have been extracted with the step size of 50 meV. The black vertical bars represent the theoretical VIEs. The CIYs are plotted with a solid red line and the photoelectron spectrum ($h\nu = 30$ eV) is plotted with a dashed black line to assist in interpretation.

Band 7 has been assigned to $(10a')^{-1}$. In Fig. 2(a), one may note that band 7 is much less intense than bands 1–6 at $h\nu = 30$ eV. The structure of band 8 is unclear, but the wide spread indicates that many-electron processes such as shake-up and correlation satellites may be involved. The inner valence region of molecules is known to break the one-electron picture due to configuration interaction and close state proximity, which induces further interference effects in the form of vibronic interactions (see, for example, Eland [47], and references therein). According to the calculations, band 8 is suggested to arise from the correlated contribution of C 2*s*, F 2*s*, and F 2*p* orbitals.

B. PEPICO—first region

The PEPICO map for electronic states between binding energies (BEs) of 12–22 eV (region 1) is presented in Fig. 3, providing an overview of the fragmentation patterns. It connects the ionic fragments to specific electron energies and thus to the internal energy changes within the molecule. The intensities have been scaled to run from 0 to 1, and black contours are set at 0.33 and 0.66. The map has been smoothed slightly for clearer visual presentation. The window of region 1 was adjusted to include the majority of the states subsequent to valence photoionization as observed in Fig. 2. For further clarity, the theoretical VIEs for these states are also shown in the CIY plots of Fig. 4.

The general trend can be examined from the map of Fig. 3, but the detailed analysis should be directed to the CIYs of Fig. 4. The parent ion $C_2H_2F_4^+$ initially stays intact at the low BE side of band 1 with the clearest trace observed at the BE of 13.0 eV, close to the calculated VIE of $17a'$ MO. As the internal energy becomes greater and a multitude of fragmentation thresholds are exceeded, the production of specific cations begins. The production of the parent molecular ion lacking one fluorine ($C_2H_2F_3^+$) is most evidently in coincidence with the electrons of bands 2 and 3, with clear emphasis on band 2.

CF_3^+, a product of the C–C bond cleavage, is detected in the whole energy range. The relative yield is found to be greatest in band 1 with minor, less emphasized production on bands 2–5. The other ionic C–C bond break product, CH_2F^+ is also detected in the whole energy range. However, the production of CH_2F^+ is heavily tending towards the higher-energy end in contrast to CF_3^+, which is in accordance with the previous study, where a different technique—photon-energy scanned TPEPICO—was employed [28].

The fragments $C_2HF_2^+$ and CHF_2^+ are also detected as minor products. $C_2HF_2^+$ is detected in coincidence with bands 3, 4, and 5, where production from band 5 is heavily preferred. For CHF_2^+, the three most pronounced structures are centered at bands 3, 4, and 5, similarly to $C_2HF_2^+$; however, band-5-related production is seen to be even more pronounced. The higher statistics of our TOF spectra (see Fig. 5) indicates that the CHF_2^+ yield is likely accompanied by some

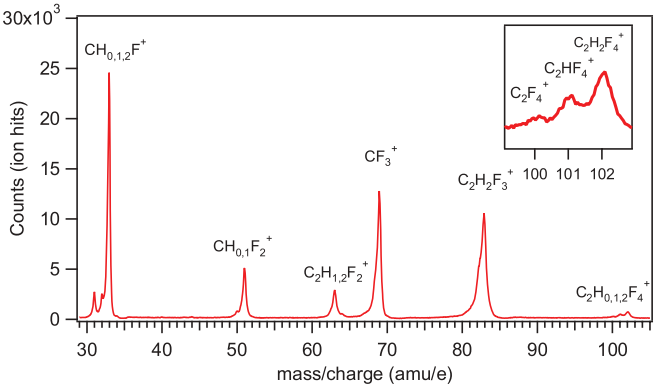

FIG. 5. (Color online) A time-of-flight mass spectrum, recorded at photon energy of 24 eV, displaying the hydrogen-loss progression of the fragments along with the major fragments directly subsequent to C–C bond fission. The small unlabeled peaks of approximately 1% relative intensity at masses of 34 and 70 u are traces of ^{13}C-containing fragments. The inset is a zoom of the low-intensity products $C_2H_{0,1,2}F_4^+$.

CF_2^+ contribution, whereas the $C_2HF_2^+$ yield is similarly accompanied by $C_2H_2F_2^+$.

A weak yield of CF^+ is also detected with band 5, with even a weaker yield within band 4. The mass peak expected from CHF^+ overlaps with that of O_2^+ (32 u). The residual gas photoelectron spectrum is dominated by H_2O^+ and N_2^+, displaying only a weak trace of the valence PES of O_2 [49], suggesting the 32 u ion to be CHF^+ by reduction. The CIY of CHF^+ was found to be extremely weak and thus it is not included in Fig. 4.

The H^+ ion was also observed at the BEs of approximately 19 to 20 eV. It is likely that this originates from H_2O's fragmentation subsequent to $(1b_2)^{-1}$ photoionization instead of band 5, as the appearance energy of H^+ from H_2O^+ is slightly below 19 eV [50]. Regarding hydrogen loss, Zhou and co-workers also calculated that the reaction CF_3–$CH_2F \rightarrow CF_3$–$CHF^+ + H + e^-$ is energetically allowed for photon energies greater than 14.09 eV, but they did not observe it [28]. However, in our TOF spectra, $C_2HF_4^+$ and $C_2F_4^+$ are both observed from 15 eV onwards, yielding crude upper limits for the appearance energies (AEs) of these fragments. A TOF spectrum is displayed in Fig. 5, demonstrating the observed hydrogen losses. Partanen *et al.* [51] have studied fluorescence emission of 1,1,1,2-tetrafluoroethane in the valence region. They observed the Balmer α and β lines due to excited hydrogen atoms, indicating (in the general level) that hydrogen loss takes place from this molecule.

C. PEPICO—second region

The PEPICO map for the second region is presented in Fig. 6, and for clarity, the separated CIYs are shown in Fig. 7. The photon energy of 45 eV is well beyond the double-ionization threshold, which has been calculated to be 35.5 eV, and thus doubly-charged ions may also be detectable. The data were gathered within a window, which includes a slight tail from band 5, the complete bands 6 and 7, and the progressively intensified structure labeled band 8. The high-energy tail of band 5 is included to demonstrate the

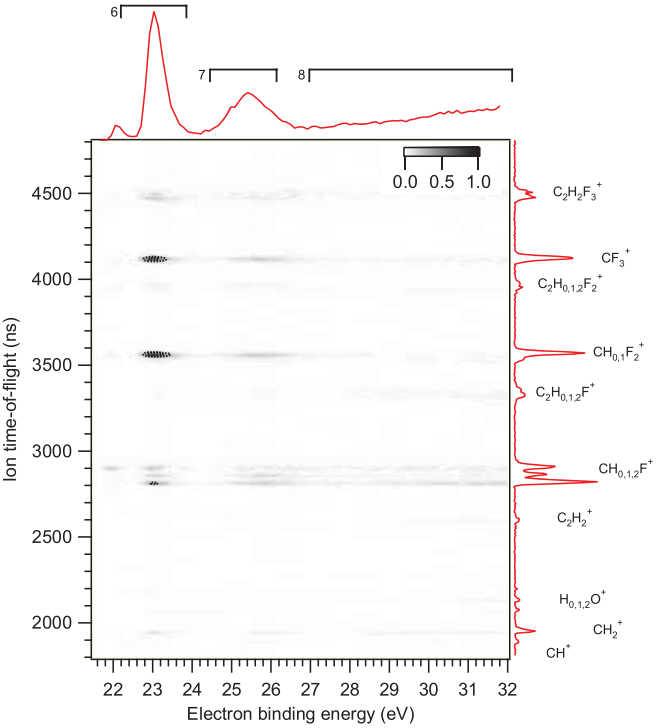

FIG. 6. (Color online) The second region PEPICO map of 1,1,1,2-tetrafluoroethane ($h\nu = 45$ eV). The dashed contour lines have been set at 33% and 66% of the maximum intensity.

difference in ion production from band 6 onwards. As can be noticed by comparing the overall fragment production of the first and second regions (Figs. 3 and 6), a greater variety of different fragments are produced in the second region. It is worth noting that the apparent split in the $C_2H_2F_3^+$ peak of Fig. 6 results from the false coincidence treatment [42] in combination with noticeable KER broadening, which appears more pronounced in comparison to the first region PEPICO experiment.

The CIYs are plotted in Fig. 7, with the exception of the extremely weak $C_2H_{0,1,2}F_2^+$ and $C_2H_2^+$. The smallest fragments, CH^+ and CH_2^+, appear below the water constituents, although the signal is faint. Other weak signals are observed for the following fragments in increasing order of time of flight: $C_2H_2^+$, $C_2H_{0,1,2}F^+$, and the previously mentioned $C_2H_{0,1}F_2^+$. As with the first region, a minor yield of H^+ was observed, but only in negligible amounts and likely originating from H_2O^+ fragmentation, as discussed before.

As can be seen from Fig. 7, the production of $C_2H_2F_3^+$ and CF_3^+ is abundant in the lower-energy region at band 6 with minor contribution to band 7. $C_2F_3^+$ appears to be nonexistent in the data. In turn, the $CH_nF_2^+$ family is not observed to appear with two hydrogens and its production is also correlated with bands 6 and 7, with CF_2^+ appearing as a less abundant shoulder on the TOF peak of this family.

The C–C bond break product CF_3^+ appears in coincidence with both bands 6 and 7. $CH_{0,1}F_2^+$ are the most abundant coincident fragments with band 6 photoionization.

The combined yield of $C_2H_{1,2}F^+$ displays only negligible fragment production from bands 6 and 7, with the majority of their yield being found at the higher-energy end of the

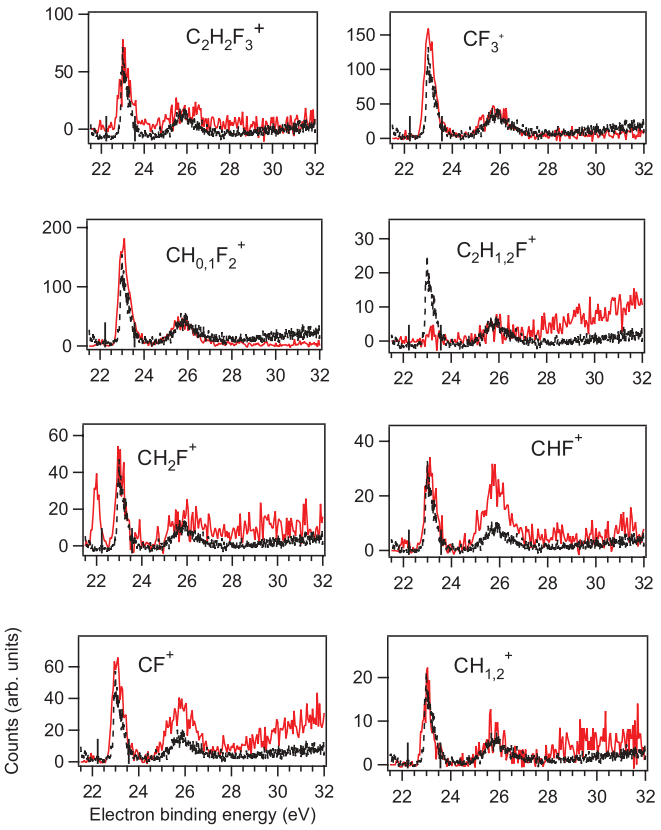

FIG. 7. (Color online) Coincident ion yields (CIYs) for the most abundant CF_3-CH_2F fragments detected subsequent to photoionization ($h\nu = 45$ eV) within the second PEPICO region. The yields have been extracted with the step size of 50 meV. The CIYs are plotted with a solid red line and the photoelectron spectrum ($h\nu = 50$ eV) is plotted with a dashed black line to assist in interpretation.

spectrum, increasing with the intensity of band 8. With $CH_{1,2}^+$, the yield is again found within bands 6 and 7, with some hints of activity from band 8.

The case of $CH_{0,1,2}F^+$ appears more complex: CH_2F^+ is initially produced subsequent to band 5 photoionization, whereas the hydrogen bond breaks resulting in CHF^+ and CF^+ appear to be energetically allowed from band 6 photoionization onwards. Production of CF^+ is also noticeably increasing towards the higher-energy end, whereas CH_2F^+ and CHF^+ production is overtaken by CF^+ at band 8. The separated yields of CH^+ and CH_2^+ display no noticeable differences: both are less abundant products observed mainly in coincidence with the band 6 and 7 photoionization.

D. Details regarding fragment identification

Zhou *et al.* [28] have determined the 298 K appearance energies (AE_{298}) from their yields. We note a general agreement between the two experiments with two exceptions: Zhou *et al.* determined the AE_{298} of CF^+ to be between 21 and 23 eV, but according to Fig. 4, it is below 21 eV, possibly even as low as 18 eV. They also report the AE_{298} for $C_2H_2F_2^+$ at 16.57(7), whereas in this experiment that ion was observed as a faint shoulder on the $C_2HF_2^+$ peak, as may be seen from Fig. 5. Zhou and co-workers note that due to their modest TOF resolution, their ion assignments may contain a false amount of hydrogen atoms, whereas our mass resolution provides the amount of hydrogens more accurately.

In our experiment, for the $C_2H_2F_2^+$ signal at the energy of 17 eV—above the previously given [28] AE_{298}—the signal is within the background fluctuation. However, $C_2HF_2^+$ is first observed at band 3, centered at 17 eV, as can be seen from Fig. 4, which leads us to believe that the ion at this TOF range is primarily $C_2HF_2^+$ with minor $C_2H_2F_2^+$ contribution (in the order of 15–20% at $h\nu = 24$ eV). Another possible explanation is that $C_2H_2F_2^+$ appears due to resonant excitation followed by autoionization, which this experiment would be unlikely to observe.

Zhou and co-workers also note [28] that above 20 eV, the CH_2F^+ peak asymmetry shows limited evidence of CHF^+ contribution. This is true according to our TOF data as well, but our spectra indicate the CHF^+ appears—very weakly—from $h\nu = 16$ eV onwards. Initially, the relative yield of CF^+ and CHF^+ with respect to CH_2F^+ is of the order of 5%. All in all, it is our understanding that the differences in the fragment identification are purely due to different TOF resolving powers between the experiments.

E. Fragmentation patterns

Some parts of the PES structure of Fig. 2 display vibrational structure indicating that the fragmentation subsequent to creation of these photoionized states occurs via predissociation [14,47], as these states are later seen to fragment. According to statistical unimolecular theories, the excess internal energy brought by photoionization is subsequently distributed between all degrees of freedom in the electronic ground state [48]. In the case of larger ionic molecules, this is typically achieved through rapid internal conversion to the electronic ground state [47]. However, in some cases, the statistical dissociation may be completely or partially overtaken when, for example, the initially excited state is directly repulsive or when the initially excited state experiences a curve crossing to a repulsive state. The PEPICO and TOF data indicate noticeable broadening in the case of $C_2H_2F_3^+$ production when inspected with least-squares fitting of Gaussian line shapes [52]. The data indicate that the decay from the second and third bands leads to C–F bond fission, in addition to other products. It is also evident from our data that over the narrow electron binding-energy window between 15 and 17.5 eV, fluorine loss dominates, with the C–C bond fission being a competing pathway. A comparison was made between the neutral-fluorine-loss peaks ($C_2H_2F_3^+$) detected in coincidence with bands 2 and 3 ($h\nu = 30$ eV). This was done by extracting the coincident ions between energy ranges specified by the approximate upper and lower electron-energy limits for the PES bands; for $C_2H_2F_3^+$, the difference in peak broadening was found to be negligible. Quantitative determination of the involved KERs is beyond the scope of this paper. However, our qualitative results support the conclusion of Zhou *et al.* regarding the observed broadening of the $C_2H_2F_3^+$ TOF peak [28]: the relative width of the neutral-fluorine-loss fragment peak indicates that a noticeable portion of the process energy is provided for the fragment's translational energy, hinting towards impulsive dissociation.

V. SUMMARY

The valence photoelectron spectrum and photofragmentation of 1,1,1,2-tetrafluoroethane have been examined by means of photoelectron, ion mass, and energy-resolved photoelectron-photoion coincidence spectroscopies. The vertical ionization energies for valence photoionized states have been calculated by employing *ab initio* methods and were found to be in good agreement with the experiment. We present experimental data on the valence structure and photofragmentation of 1,1,1,2-tetrafluoroethane. A tentative assignment of the outer valence singly-ionized states was presented on a theoretical and experimental basis. The photofragmentation pathways were inspected and compared to the literature [28] and reasonable agreement was found: the MO labeling produced by our calculations was otherwise identical, with the exception of two orbitals switching places ($16a'$ and $7a''$). In addition, the increased ion mass resolution allowed us to more clearly identify the fragments observed subsequent to outer valence photoionization. The outer valence and inner valence photofragmentation were also inspected with PEPICO spectroscopy, where we identified the observed fragments and presented their coincident yields as a function of electron binding energy. In the inner valence region, assumed to consist of heavily correlating states, a multitude of different cationic products was identified, displaying greater variety over the fragmentation resulting from outer valence photoionization.

ACKNOWLEDGMENTS

This work has been financially supported by the Research Council for Natural Sciences and Engineering of the Academy of Finland. The research leading to these results has received funding from the European Community's Seventh Framework Programme (FP7/2007-2013) under Grant Agreement No. 226716. J.A.K. acknowledges the Vilho, Yrjö and Kalle Väisälä Foundation. A.S. acknowledges financial support from the Swedish Research Council and the Research Council for Natural Sciences of the Academy of Finland. S.U. would like to acknowledge the Research Council for Natural Sciences and Engineering of the Academy of Finland (Grant No. 135871) and Lund University for financial support. In addition, the authors thank E. Kukk for general support and the original macros used for coincidence data handling. The staff at MAX-lab are also acknowledged for their assistance during the experiments.

[1] C. H. Jackman, M. T. DeLand, G. J. Labow, E. L. Fleming, D. K. Weisenstein, M. K. W. Ko, M. Sinnhuber, and J. M. Russell, J. Geophys. Res. **110**, A09S27 (2005).
[2] A. M. Holloway and R. P. Wayne, *Atmospheric Chemistry* (Royal Society of Chemistry, Cambridge, 2010).
[3] A. McCulloch, P. M. Midgley, and P. Ashford, Atmos. Environ. **37**, 889 (2003).
[4] J. S. Fransisco and M. M. Maricq, Acc. Chem. Res. **29**, 391 (1996).
[5] G. J. M. Velders, D. W. Fahey, J. S. Daniel, M. McFarland, and S. O. Andersen, Proc. Natl. Acad. Sci. **106**, 10949 (2009).
[6] K. P. Shine and W. T. Sturges, Science **315**, 1804 (2007).
[7] D. J. Hofmann, J. H. Butler, E. J. Dlugokencky, J. W. Elkins, K. Masarie, S. A. Montzka, and P. Tans, Tellus B **58**, 614 (2006).
[8] S. A. Montzka, E. J. Dlugokencky, and J. H. Butler, Nature (London) **476**, 43 (2011).
[9] T. J. Wallington and W. F. Schneider, Faraday Discuss. **100**, 55 (1995).
[10] S. Pinnock, M. D. Hurley, K. P. Shine, T. J. Wallington, and T. J. Smyth, J. Geophys. Res. **100**, 23227 (1995).
[11] http://eur-lex.europa.eu/LexUriServ/site/en/oj/2006/l_161/l_16120060614en00120018.pdf
[12] L. J. Butler and D. M. Neumark, J. Phys. Chem. **100**, 12801 (1996).
[13] Y.-P. Lee, Annu. Rev. Phys. Chem. **54**, 215 (2003).
[14] H. Sato, Chem. Rev. **101**, 2687 (2001).
[15] J. H. D. Eland, Laser Chem. **11**, 259 (1991).
[16] B. N. McMaster, Mass Spectrom. **3**, 1 (1975).
[17] M. N. Piancastelli, W. C. Stolte, G. Öhrwall, S.-W. Yu, D. Bull, K. Lantz, A. S. Schlachter, and D. W. Lindle, J. Chem. Phys. **117**, 8264 (2002).
[18] E. Kukk, M. Huttula, J. Rius i Riu, H. Aksela, and S. Aksela, J. Phys. B **37**, 2739 (2004).
[19] W. C. Stolte, R. Guillemin, S.-W. Yu, and D. W. Lindle, J. Phys. B **41**, 145102 (2008).
[20] M. Schwell, H.-W. Jochims, H. Baumgärtel, and S. Leach, Chem. Phys. **353**, 145 (2008).
[21] J. L. Franklin, P. M. Hierl, and D. A. Whan, J. Chem. Phys. **47**, 3148 (1967).
[22] J. Laskin and C. Lifshitz, J. Mass. Spec. **36**, 459 (2001).
[23] B. Bapat and V. Sharma, Int. J. Mass Spectrom. **251**, 10 (2006).
[24] R. E. Continetti, Annu. Rev. Phys. Chem. **52**, 165 (2001).
[25] C. Miron and P. Morin, Nucl. Instrum. Methods Phys. Res., Sect. A **601**, 66 (2009).
[26] T. Baer, Int. J. Mass Spectrom. **200**, 443 (2000).
[27] W. Zhou, D. P. Seccombe, R. Y. L. Chim, and R. P. Tuckett, Surf. Rev. Lett. **9**, 153 (2002).
[28] W. Zhou, D. P. Seccombe, and R. P. Tuckett, Phys. Chem. Chem. Phys. **4**, 4623 (2002).
[29] F. Aquilante, L. De Vico, N. Ferré, G. Ghigo, P.-Å. Malmqvist, P. Neográady, T. B. Pedersen, M. Pitonak, M. Reiher, B. O. Roos, L. Serrano-Andrés, M. Urban, V. Veryazov, and R. Lindh, J. Comput. Chem. **31**, 224 (2010).
[30] S. Papasavva, K. H. Illinger, and J. E. Kenny, J. Phys. Chem. **100**, 10100 (1996).
[31] S. Papasavva, S. Tai, A. Esslinger, K. H. Illinger, and J. E. Kenny, J. Phys. Chem. **99**, 3438 (1995).
[32] T. Ogata and Y. Miki, J. Mol. Struct. **140**, 49 (1986).
[33] S. Urpelainen, M. Huttula, T. Balasubramanian, R. Sankari, P. Kovala, E. Kukk, E. Nommiste, S. Aksela, R. Nyholm, and H. Aksela, AIP Conf. Proc. **1234**, 411 (2010).

[34] M. Huttula, S. Heinäsmäki, H. Aksela, E. Kukk, and S. Aksela, J. Electron Spectrosc. Relat. Phenom. **156–158**, 270 (2007).
[35] M. Huttula, M. Harkoma, E. Nommiste, and S. Aksela, Nucl. Instrum. Methods Phys. Res., Sect. A **467**, 1514 (2001).
[36] A. W. Potts and W. C. Price, Proc. Roy. Soc. A **326**, 181 (1972).
[37] J. A. R. Samson and W. C. Stolte, J. Electron Spectrosc. Relat. Phenom. **123**, 265 (2002).
[38] A. Fahlman, M. O. Krause, T. A. Carlson, and A. Svensson, Phys. Rev. A **30**, 812 (1984).
[39] J. Niskanen, S. Urpelainen, S. Aksela, H. Aksela, O. Vahtras, V. Carravetta, and H. Ågren, Phys. Rev. A **81**, 043401 (2010).
[40] E. Kukk, K. Kooser, D. T. Ha, S. Granroth, and E. Nõmmiste, J. Phys. B **43**, 065103 (2010).
[41] G. Prümper and K. Ueda, Nucl. Instrum. Methods Phys. Res., Sect. A **574**, 350 (2007).
[42] E. Kukk, R. Sankari, M. Huttula, A. Sankari, H. Aksela, and S. Aksela, J. Electron Spectrosc. Relat. Phenom. **155**, 141 (2007).
[43] K. Andersson, P.-Å. Malmqvist, B. O. Roos, A. J. Sadlej, and K. Wolinski, J. Phys. Chem. **94**, 5483 (1990).
[44] K. Andersson, P.-Å. Malmqvist, and B. O. Roos, J. Chem. Phys. **96**, 1218 (1992).
[45] J. Olsen, B. O. Roos, P. Jørgensen, and H. J. Aa. Jensen, J. Chem. Phys. **89**, 2185 (1988).
[46] B. O. Roos, P. R. Taylor, and P. E. M. Siegbahn, Chem. Phys. **48**, 157 (1980).
[47] J. H. D. Eland, *Photoelectron Spectroscopy*, 2nd ed. (Butterworths, London, 1984).
[48] P. B. Armentrout and T. Baer, J. Phys. Chem. **100**, 12866 (1996).
[49] O. Edqvist, E. Lindholm, L. E. Selin, and L. Åsbrink, Phys. Scr. **1**, 25 (1970).
[50] K. Norwood, A. Ali, and C. Y. Ng, J. Chem. Phys. **95**, 8029 (1991).
[51] L. Partanen *et al*., unpublished.
[52] E. Kukk, computer code SPANCF, http://www.physics.utu.fi/en/research/material_science/Fitting.html (2009).